Synthesis and Characterization of Activated Carbon Derived from Agricultural Waste (Cocoa Pod Husks) as Potential Electrode for Symmetric Supercapacitor

Oladepo Fasakin[a,b*], Kabir O. Oyedotun[b],Abdulmajid A. Mirghni[b], Ndeye F. Sylla[b], Badr A. Mahmoud[b], Ncholu Manyala[b*]

[a]Department of Physics and Engineering Physics, Obafemi Awolowo University, Ile-Ife 220005, Nigeria

[b]Department of Physics, University of Pretoria, Pretoria 0002, South Africa

*Corresponding author's emails: fasakinoladepo@oauife.edu.ng, Tel.: + (234)8030786404
ncholu.manyala@up.ac.za, Tel.: + (27)12 420 3549

Highlights

- Activated carbon derived from Cocoa pod husk is synthesized via tube furnace with KOH as activating agent.
- 2.5 M KNO_3, 1 M Na_2SO_4, and 1 M $NaNO_3$ are examined as potential neutral electrolytes.
- A specific capacitance of ~168 F g^{-1} is recorded for ACC 600 °C at 0.5 Ag^{-1} in 2.5 M KNO_3.
- The material's unique stability and energy density display its efficacy as electrode for energy storage applications.

Abstract

Biomass waste of cocoa pod husks is adopted as starting material to synthesize Activated carbon (ACC) using a tube furnace via KOH activation with temperature ranging from 500 °C to 800 °C. The activated carbon prepared at 600 °C (ACC 600 °C) shows improved qualities than the other prepared samples, according to the physico-chemical analyses. A sponge-like morphology, amorphous structure, and microporous and mesoporous carbon are observed in the synthesized material. Trasatti approach is adopted to verify the storage mechanism of the activated carbon material (ACC 600 °C) with the percentage contribution of capacitive and diffusion-controlled effect as 92.4732% and 7.5268% for positive electrode while the negative electrode possesses 75.565% and 24.435% at scan rate of 50 mVs^{-1}. A symmetric device is fabricated from the ACC 600 °C, which gives a maximum specific energy (S.E.) of 19 Wh kg^{-1} with a corresponding specific power (S.P.) of 453 W kg^{-1} at a specific current of 0.5 A g^{-1} in 2.5 M KNO_3 solution. The coulombic efficiency of the device is 99.6% after 10000 cycles with 72% capacitance retention. The obtained results suggest that the activated carbon derived from cocoa pod husks could be used as a promising material for supercapacitor's application.

Keywords: Biomass; Cocoa pod husk; Activated carbon; Specific energy; Supercapacitor

1. Introduction

The ever-increasing demand of the use of energy storage devices across the globe is worth searching for a cheap or possibly free (waste) biomass material to replace some of expensive electrode materials for fabrication of electrodes for supercapacitors. Roughly 10% of the energy utilized worldwide is made up of biomass, which comes from a wide variety of agricultural leftovers [1]. To find materials for energy applications that are plentiful, renewable, and sustainable, one must go in this direction [2]. It has been determined that using fossil fuels, among other things, is not sustainable over the long term, particularly considering the primary threat that global warming poses to life as we know it due to greenhouse gas emissions [3]. Because of its detrimental effects on the environment, research is being done to find new, safe, dependable, and clean alternative energy sources [4]. A lot of interests have been shown in the creation of novel, scalable and adaptable energy storage systems, such as battery-type charge storage, pseudocapacitive charge storage, and double-layer charge storage, to meet the challenges for rising needs of energy storage materials [5]. Of these storage mechanisms, electrochemical double layer capacitors (EDLCs) have the most potential for use in a variety of applications, such as hybrid electric vehicles, regenerative braking systems, portable electronics, load levelling, uninterruptible power sources, and so on because of their quick charging and discharging mechanism, exceptional long-life cycle, and high-power density [6,7].

A wide range of nanostructured materials containing carbon, including activated carbon (AC) [8], carbon nanotubes (CNTs) [9,10], carbide-derived carbons (CDCs) [11], onion-like carbons (OLCs) [12,13], and graphene [14,15] are available in different shapes and can be used as electrode materials for the upcoming generation of supercapacitors. A lot of literatures had been reported earlier in the synthesis of porous carbon from agricultural biomass for the fabrication of symmetric and asymmetric devices [[16], [17], [18]]. For example, using KOH and ZnCl2 as activating agents, activated carbon was synthesized by V. Subramanian et al. [19] using banana fibres that had better porosity. After testing the material in 1 M Na_2SO_4 within a 1 V potential window, a specific capacitance of 74 F g^{-1} was measured. Zhang et al. used KOH and rice husk as activating agent and precursor, respectively, to prepare porous carbon with 352 F g^{-1} specific capacitance at 1 A g^{-1} [20] Ramzi et al. used KOH/NaOH to activate olive husks and the synthesized hierarchical porous carbons manifested a specific capacitance of 549 F g^{-1} at 0.5 A g^{-1} [21,22]. Also, Venkatesan et al. reported that raw leather trimming waste derived nitrogen self-doped activated carbon was prepared by chemical activation using KOH and it showed a high specific surface area with a micro/mesoporous nature. The resulting porous texture helps with the penetration of electrolyte improved the rate performance and yielded good cycle stability of 91 % over 10,000 cycles at 10 A g^{-1}. The fabricated symmetric pouch cell in an aqueous electrolyte revealed extraordinary energy and power densities of 3.7 Wh kg^{-1} at 0.5 A g^{-1} and the power density of 4968 W kg^{-1} at 10 A g^{-1} [23]. In a more recent development, X. He and colleagues also employed rice husks as a precursor material to create high-performance porous carbons for SCs [24]. For their investigation, a material with a specific surface area of 1442 m^2 g^{-1} was acquired, and it was tested in 6 M KOH aqueous electrolyte. At a specific current of 2 A g^{-1}, the material demonstrated up to 95.1% capacitance retention of its initial capacitance. Other comparisons of various agricultural waste derived activated carbon materials were reported in literature and as presented in Table 1.

Table 1. Physical properties of ACC samples.

Samples	SSA (m^2/g)	PV (cc/g)
ACC 500°C	300	0.163
ACC 600°C	585	0.648
ACC 700°C	836	0.571
ACC 800°C	747	0.433

Table 2. Comparing the current study's findings with electrodes made from biomass carbon.

Origin of electrode materials	Electrolyte	Specific Current (Ag^{-1})	S.E ($Whkg^{-1}$)	S.P ($W kg^{-1}$)	Type of device	Reference
Sunflower seed shell	3 M KOH	0.5	4.8	240	Symmetric cell	[47]
Oil palm empty fruits bunch	6 M KOH	0.5	5.11	230	Symmetric cell	[48]
Rice straw	1 M H_2SO_4	0.5	7.8	150	Symmetric cell	[49]
Coconut shell	Polymer gel electrolyte	0.5	11	325	Symmetric cell	[50]
Banana peels	1 M $NaNO_3$	0.5	18.6	485	Symmetric cell	[34]
Bean seedpod	1 M KOH	0.5	10.58	720	Symmetric cell	[51]
Marula nutshell	2.5 M KNO_3	0.5	17.2	448.7	Symmetric cell	[52]
Cocoa pod husks	2.5 M KNO_3	0.5	19	453	Symmetric cell	This work

In this work, a novel sponge-like and porous carbon has been synthesized from cocoa pod husks, of which its electrochemical properties were investigated and reported in a symmetric device using suitable neutral electrolyte (2.5 M KNO_3) in both three and two-electrode configurations. In recent years, cocoa pod husks and other agricultural waste had been converted into activated carbon majorly for energy storage [25,26] and water treatment [[27], [28], [29]], which had been previously reported in the literature. Herein, cocoa pod husks precursor was initially pre-carbonized in an oven in a low acidic medium. The hydrochar was ground and activated with (Potassium hydroxide) KOH in a ratio of 1:1 and later carbonized at temperature variation of 500–800 °C (ACC 500°C, ACC 600°C, ACC 700°C and ACC 800 °C) using a tube furnace. Analyses of the samples revealed that the ACC 600 °C exhibited novel properties such as sponge-like morphology, porous and improved electrochemical performances compared to the other ACC samples. The prepared activated carbon had earlier been reported as negative electrodes for asymmetric devices in some of our recently published works [17,[30], [31], [32], [33]]. Hence, this work basically presents physico and electrochemical properties of the material and its symmetrical arrangement as a potential electrode for supercapacitor's application.

2. Experimental details

2.1. Synthesis of activated carbon from cocoa pod husks

Scheme 1 shows the synthesis process of activated carbon from cocoa pod husk waste that was sourced from agricultural farm at Obafemi Awolowo University, Ile–Ife, Nigeria. The methodology adopted is like the work earlier reported [34]. In summary, 100 ml of distilled

water (D.W) combined with 0.5 M H_2SO_4 (10 ml), was added to crushed cocoa pod husks in a 120 ml autoclave and pre-carbonized in an oven for 12 h at 160 °C. By-product was filtered and dried in an oven at 60 °C for 48 h. Afterwards, 10 g of the by-product was then mixed with potassium hydroxide pellet (1:1 mass ratio) in an agate mortal and carbonized in a tube furnace at 600 °C, 5 ºC/min under argon gas atmosphere for 1 h. Thereafter, the recovered activated sample was soaked overnight in a 3 M HCl solution to neutralize any residual KOH in the sample, then followed by washing several times with de-ionized water until a pH of 7 was attained. The sample was then allowed to dry overnight at 60 °C in an ambient oven. The same procedure was repeated at temperatures ranging from 500 to 800 °C.

Scheme 1. Schematic representation for the synthesis of activated carbon from cocoa pod husks.

2.2. Characterization of activated carbon from cocoa pod husks

The morphologies of the carbon materials were examined using a field emission scanning electron microscope (FESEM) (Zeiss Ultra Plus 55 field emission) running at 2.0 kV. The detailed morphology was determined by using transmission electron microscopy (TEM) (JEOL JEM-2100F microscope) at 200 kV. The sample (ACC 600 °C) with novel property was dissolved in 99% ethanol and put onto on a lacey copper grid for analysis. An Ulm, Germany-based WITec confocal Raman microscope (WITec alpha 300 RAS+) with a laser wavelength of 523 nm, laser power of 4 mW, and spectrum acquisition time of 120 s was also used to determine defects and graphitization in the samples. A PANalytical BV, Netherlands, XPERT-PR. O diffractometer (XRD) running with $\lambda = 1.789$ A at 35 kV and 50 mA was used to characterize the structural characteristics of ACC samples. However, each of the prepared samples was vacuum-degassed for nearly 12 h at 100 °C before being measured using Quantachrome (NOVAtouch NT 2LX-1, Volts 220, USA), which ran Quantachrome Tourch Win Software Version: 1.22, to determine the pore size distribution and specific surface area of the ACC samples.

2.3. Measurement of electrochemistry

A multichannel VMP300 potentiostat (Bio-Logic, France) was used to conduct the electrochemical measurements at room temperature. 80 wt percent of the active ingredient, 10 wt percent polyvinylidene fluoride (PVDF), and 10 wt percent carbon black were blended in a few drops of N-methyl-2-pyrrolidone (NMP) and coated on a 1×1 cm^2 and 16 mm (diameter) nickel foam for three and two electrode measurements, respectively. The generated electrode was subsequently vacuum-dried for 12 h at 80 °C in an electric oven to ensure complete NMP evaporation. For the electrochemical testing of the ACC electrodes in three different electrolytes (1 M $NaNO_3$, 1 M Na_2SO_4, and 2.5 M KNO_3), glassy carbon plate served as the counter electrode and Ag/AgCl (3 M KCl) as the reference electrode. For all three electrode samples, the mass loading of each electrode was kept at around 2.8 mg/cm^2, and for the full device, it was 4.5 mg/cm^2.

The symmetric device was put together in CR2032-type coin cells with two electrodes spaced apart by 0.18 μm filter paper. The device's galvanostatic charge-discharge (GCD) and cyclic voltammetry (CV) measurements were recorded at different scan rates and particular currents within a cell potential spanning from 0 to 1.8 V. Electrochemical impedance spectroscopy (EIS) studies in an open circuit potential and frequency range of 100 kHz to 0.01 Hz were carried out using a sinusoidal signal of 5 mV.

For three-electrode measurements, the gravimetric capacitance was calculated as stated in equation (1):

$$C_{1/2} = \frac{\mathrm{I}\Delta\mathrm{t}}{\mathrm{m}\Delta\mathrm{V}} \tag{1}$$

The gravimetric capacitance (F g^{-1}) for two-electrode was also calculated according to equation (2):

$$C_g = \frac{4\mathrm{I}\Delta\mathrm{t}}{\mathrm{M_T}\Delta\mathrm{V}} \tag{2}$$

in two-electrode configuration, the charge is equally divided over two capacitors in series, is accounted for by the factor of 4.

Equation (3) provides an estimate of the device's specific energy (S.E), E_8 (Wh/kg):

$$E_s = \frac{\mathrm{C}(\Delta\mathrm{V})^2}{28.8} \tag{3}$$

While the corresponding specific power (S.P), P_8 (W/kg) was deduced in line with equation (4):

$$P_s = 3600\frac{E_s}{\Delta\mathrm{t}} \tag{4}$$

Using the charge-discharge curve, the coulombic efficiency (C.E.) was calculated by equation (5):

$$C.E = \frac{\Delta\mathrm{t_{discharge}}}{\Delta\mathrm{t_{charge}}} \tag{5}$$

where ΔV is working potential (V), I, is applied current (mA), m (mg) is the total mass of the active material, M_T is the total mass of the device's positive and negative electrodes, and Δt (s) is discharge time.

The mechanism of energy storage of the electrode material (ACC 600 °C) is further studied according to the CV curves at different scan rates via the electrochemical reactions by examining the relation of the current ($\imath$) with scanning rate (v), according to power law [35,36]

$$i = av^b \tag{6}$$

$$\log(i) = \log(a) + blog(v) \tag{7}$$

Where *a* and *b* are parameters which could be extracted through the linear relationship from equation (7). Equation (7) can also be compared with equation graph

In addition, the contribution proportion of capacitive and diffusion-controlled effect is also determined by using Trasatti approach.

$$C = \frac{k}{\sqrt{v}} + C_o \tag{8}$$

Where k is a constant, *v* is the scan rate, *C* is the capacitance of the electrode at a given scan rate and C_0 is the capacitance of EDLC

Taking the reciprocal of Equation (8),

$$\frac{1}{C} = k\sqrt{v} + \frac{1}{C_o} \tag{9}$$

$$\left(\frac{1}{C_o}\right)^{-1} = C_T \tag{10}$$

Where C_T is the total capacitance of the electrode at a given scan rate

$$\%\ \text{Capacitive} - \text{controlled effect} = \frac{C_o}{C_T} \times \frac{100}{1} \tag{11}$$

$$\%\ \text{Diffusion} - \text{controlled effect} = 100 - \%\ \text{Capacitive} - \text{controlled effect} \tag{12}$$

At lower magnification, Fig. 1(a–d) shows the morphologies of activated carbon synthesized from wasted cocoa pod husks at different temperatures ranging from 500 to 800 °C. In Fig. 1a, the micrograph depicted that the surface of the sample prepared at 500 °C was partially activated and rough, indicating that the material was not completely activated. As the temperature increased, the surface of the activated carbon prepared at 600 °C (Fig. 1b) gave a remarkable morphology that was sponge-like in nature with cavities. Also Fig. 1c showed similar surface with less cavities and Fig. 1d showed mutilated flakes, confirming low quality of activated carbon present.

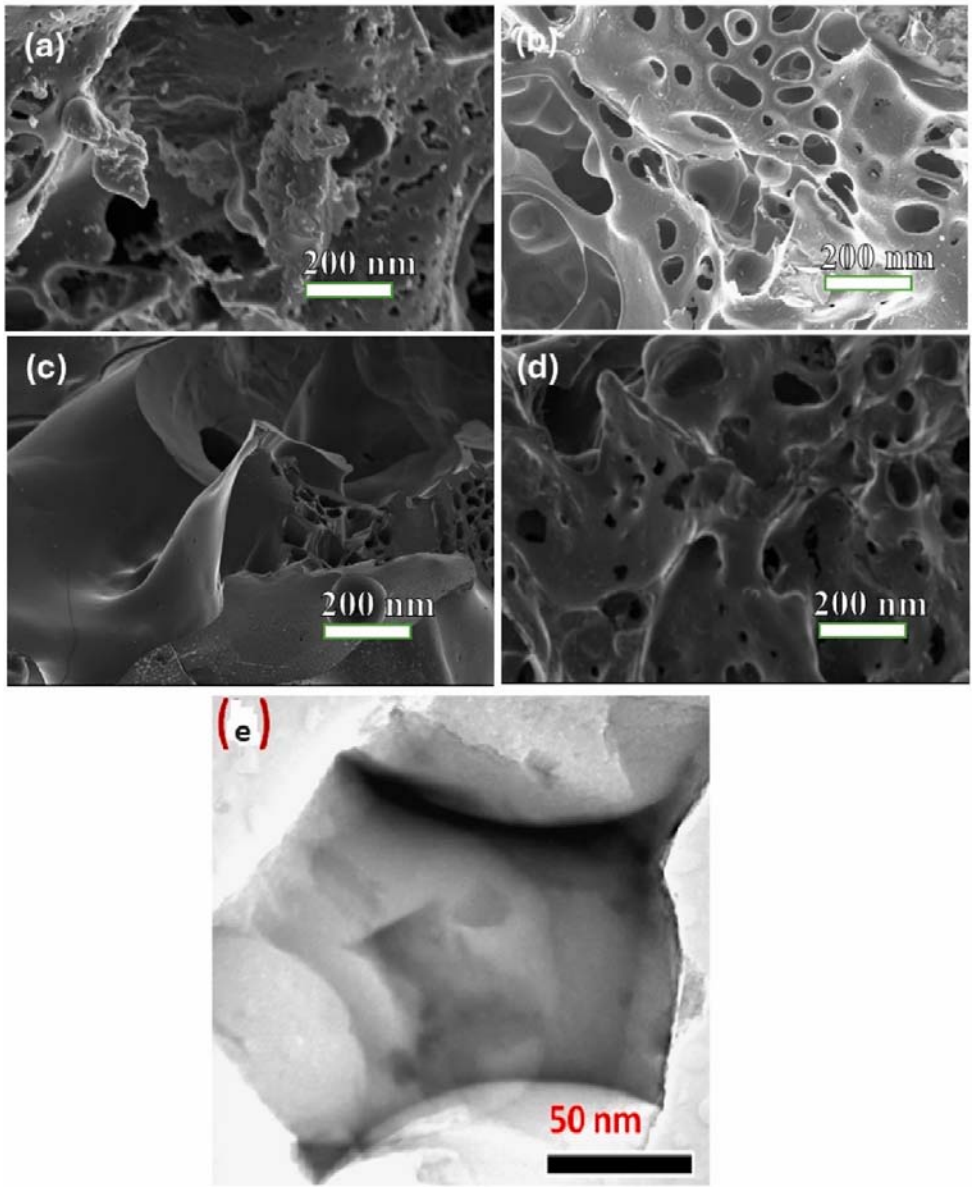

Fig. 1. SEM images of activated carbon derived from cocoa pods husk (ACC) carbonized at different temperature: (a) 500 °C (b) 600 °C (c) 700 °C and (d) 800 °C (e) TEM image of porous activated carbon derived from cocoa pod husks at temperature 600 °C.

The ACC materials' SEM images are displayed in Fig. 1. It is evident from the figure that the KOH activation causes cavities to form, and that these cavities contain a significant number of pores that are closely linked within the structures of the materials in a three-dimensional manner. At higher activation temperatures, a deformed fine structure was seen (Fig. 1(c and d)). At higher magnification, TEM image (1(e)) depicted a network of interconnected 3D hollows that overlap, which could be advantageous for applications involving energy storage. Fig. S1 also showed the surface of the activated carbon at a very high magnification. Figure S2 (a –c) reveals the elemental mapping of Activated Carbon sample (ACC 600 °C) displaying the uniform distribution of carbon, oxygen, and silicon, respectively. Figure S2 (d) indicates the percentage of these elements composition which are 89.7, 10.1, 0.2, respectively. The presence of silicon could come from ashes in the activated carbon sample, though it is very

small. Structurally, Fig. 2(a & b) shows Raman and X-ray diffraction spectra of activated carbon derived from cocoa pod husks at different carbonization temperature ranging from 500 to 800 °C. The Raman spectra for all four samples were compared with signatory D- and G-peaks centered at a wavenumber of 1341 and 1589 cm^{-1} respectively (see Fig. 2a). This confirms a high structurally disordered 3D carbon material created from the biomass raw material [[37], [38], [39], [40], [41], [42]]. The D and G peaks are attributed to defect and graphitization of the sample, respectively. The shown 2D peaks in the range of 2500–3500 cm^{-1} for the samples indicate the presence of ordered sp^2 carbon regions, which is due to the presence of graphitic microdomains within the amorphous matrix as a result of high temperatures adopted in the activation of the samples. To determine the density of flaws or the degree of crystallization in carbon materials, the intensity ratio D peak to G peak (I_D/I_G) is used. The estimated I_D/I_G for the ACC 500, ACC 600, ACC 700, and ACC 800 samples are 0.99, 0.99, 1.00, and 0.99, respectively, indicating that the as-prepared samples are amorphous in nature [43]. Structurally, the samples had diffraction peaks at high magnification (700 and 800 °C) that do not correspond to the graphite ICSD card 31170 with a space-group of $P6_3mc$ but a notable broader peak at roughly 30.5° was seen at low carbonization temperatures (600 °C). This suggests a high degree of disorder in the ACC materials, which translating to high degree of amorphous state in the sample. The starting temperature (500 °C) gave a similar structure, but carbon peak was not clearly prominent in the sample. This could be as a result of partial and incomplete carbonization that occurred during the sample preparation as seen in Fig. 2b. XRD confirmed structural analysis of carbonaceous materials. The observed enhanced sharpness of the 30.5° peak in the amorphous ACC700 and ACC800 activated carbon, respectively, indicates the presence of ordered graphitic domains, within the amorphous matrix. These regions are larger and less strained compared to the rest of the materials, leading to sharper diffraction peaks.

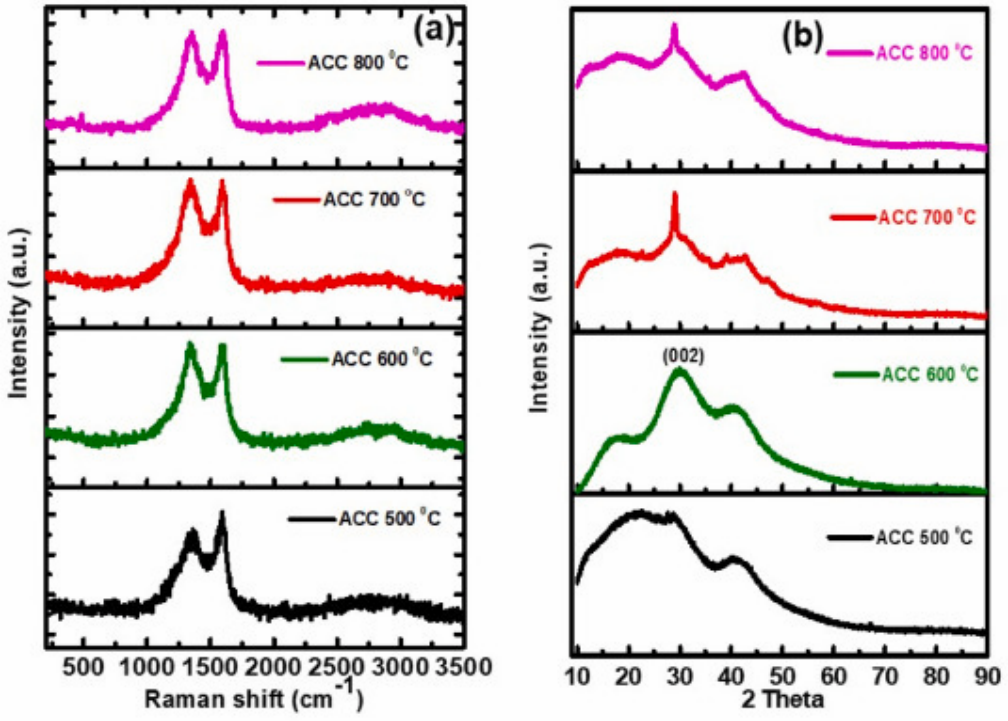

Fig. 2. (a) Raman and (b)X-ray diffraction spectra of activated carbon derived from cocoa pod husks (ACC) at temperatures ranging from 500 to 800 °C.

Fig. 3a,b shows the pore size distribution and N_2 adsorption/desorption isotherms of the carbonized ACC samples. As seen in Fig. 3a, all isotherms at high relative pressure (P/P0) present type-II behavior with H4 hysteresis loop indicating complex material containing both micropores and mesopores [2]. At 500, 600, 700, and 800 °C, the specific surface areas (SSA) and pore volume (PV) of the carbonized materials were measured, and their details are shown in Table 1. In Fig. 3a, the SSA was observed to increase with increasing temperature except at ACC 800 °C. Peaks in all the samples showed the presence of micro-pores and mesopores and that were clearly visible in Fig. 3b. In Fig. 3c, the sample ACC 600 °C with SSA of 585 $m^2\ g^{-1}$ and pore volume 0.648 cc/g is preferable for supercapacitor's application. From the data in Tables 1 and it is seen that the specific surface area values initially increase with increasing carbonization temperature from 500 to 700 °C but decrease as the temperature further increases to 800 °C. This is linked to average pore size enlargement effect shown in the average pore diameter values reported from the BET results in Table 1. This strange behavior had been observed and reported in our previous works [43,44]. By physical inspection of the micrographs in Fig. 1 (b), the sample prepared at 600 °C possessed visible cavities that look like sponge which could be responsible for high pore volume as recorded by Braunner Emmett Teller result and which may translate to better electrochemical performance of the sample.

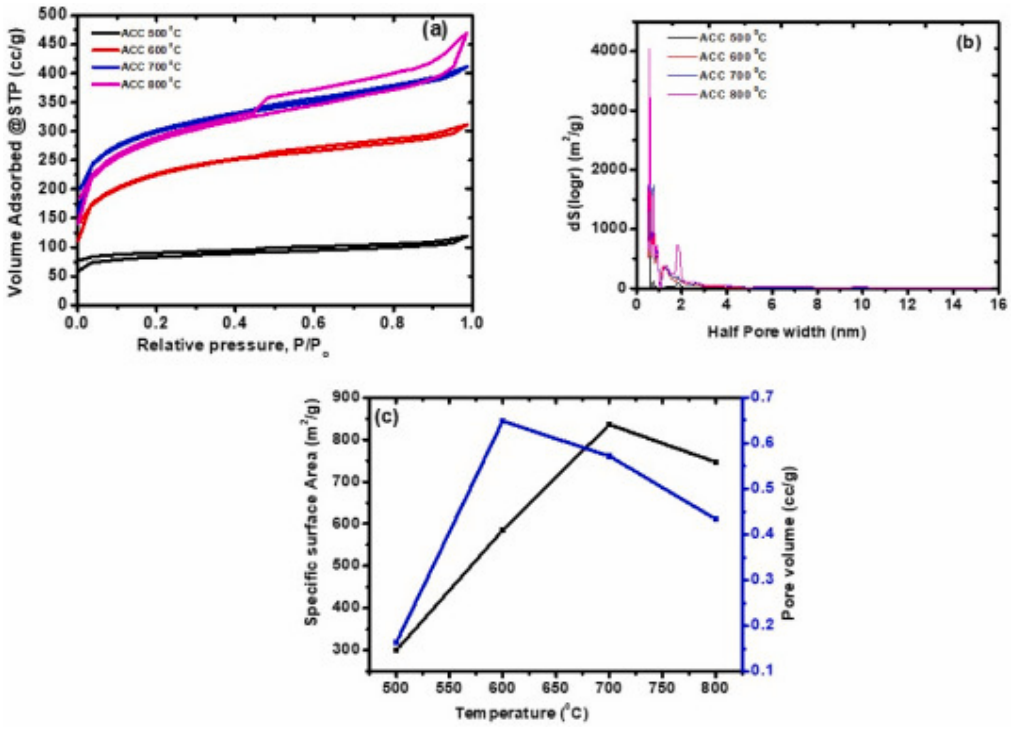

Fig. 3. (a) N_2 physisorption of activated carbon derived from cocoa pod husks (ACC) at different temperature, ranging from 500 to 800 °C (b) The plot of pore size distribution, and (c) pore volume and specific surface area against temperature for the ACC samples.

This is ascribed to its higher cyclic voltametric curve and shorter diffusion length as compared to other samples in 2.5 M KNO_3 electrolyte (see Fig. 4).

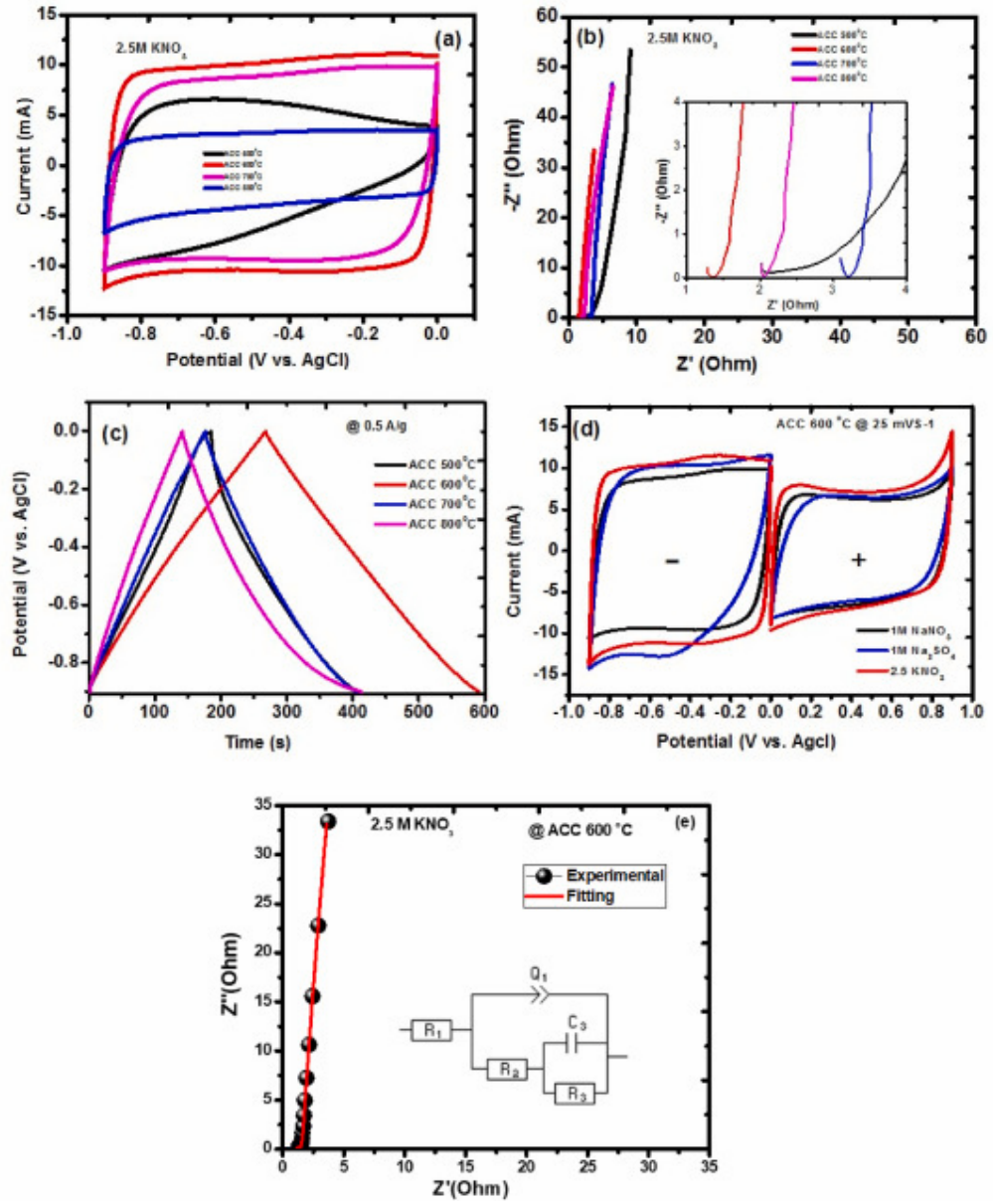

Fig. 4. (a) CV plots of the activated carbon of cocoa pod husks at different temperature (b) associated EIS of the samples (inset shows an enlarge image of high frequency region in Fig. 4(b)), (c) GCD plots of various ACC electrodes at 0.5 Ag^{-1} and (d) CV of the best sample (ACC 600°C) at both potential windows tested in three different neutral electrolytes.(e) equivalent circuit of EIS analysis for three electrode configurations of the best sample (ACC 600°C).

Fig. 4 (a) shows plots of CV curves at 25 mV s^{-1} for ACC materials, which were synthesized between the temperature of 500 °C and 800 °C and tested in the same neutral electrolyte (2.5 M KNO_3). Amongst the carbonization temperature, the temperature at 600 °C exhibits higher current response at negative potential of 0.9V than other temperatures as shown in Fig. 4 (a). For the ACC materials evaluated in neutral electrolytes, the CV rectangular shapes demonstrate excellent capacitive behavior, suggesting that all the samples showed electric double-layer storage mechanism. The carbonization temperature significantly influences the electrochemical behavior of electrode materials, and the appropriate electrolyte used [28]. To further investigate best and improved sample among the four ACC materials, corresponding

EIS was also carried out on each sample as shown in Fig. 4 (b). Equivalent series resistances (ESRs) of the ACC materials were measured in 2.5 M KNO_3 giving the values of 2.72 Ω, 1.34 Ω, 2.02 Ω, and 3.14 Ω for ACC 500°C, ACC 600°C, ACC 700°C and ACC 800 °C, respectively. The ACC 600 °C electrode was noted to show the lowest ESR, indicating the electrode's higher conductivity compared to others. The electrode's total power performance and energy efficiency are limited by the ESR's magnitude [5]. The ACC 600 °C electrode's shorter ion diffusion path within the electrolyte accounts for its better electrochemical performance [2] when compared to the other electrodes. This agrees with Fig. 4a which shows a highest current response as indication of good interaction between the electrolyte and electrode at the electrolyte/electrode interface. It is to be noteworthy that the physical properties such as sponge-like surface with cavities revealed by FESEM and a network of interconnected 3D hollows as clearly shown in TEM, amorphous structure from XRD indicating quality activated carbon, presence of defect and graphitization in Raman spectrum, and high pore volume of N_2 physisorption measurement, are all pointing to the fact that the sample ACC 600 °C possesses unique properties that are novel, which could be responsible for the better electrochemical performance of the electrode as shown in Fig. 4(a and b). Fig. 4c further shows the GCD curves of various electrodes at specific current of 0.5 A/g. It is evident that ACC 600 °C sample exhibits longer discharge time than other electrodes. The fact that ACC 600 °C sample shows superior electrochemical results led us to investigate the electrode in different neutral electrolytes as ACC electrode can respond differently in different electrolytes. Hence, this is to establish which neutral electrolyte our best will perform. Therefore, Fig. 4d displays the capability of (ACC 600 °C) electrode material in three (2.5 M KNO_3, 1 M Na_2SO_4, and 1 M $NaNO_3$) neutral electrolytes, to elucidate its possibility to work in positive and negative potentials and determine the most appropriate neutral electrolyte for symmetric device. It is shown that 2.5 M KNO_3 electrolyte, shows a higher current response in both positive and negative potential windows as clearly shown in Fig. 4 (d) as compared to other electrolytes. Fig. 4 (e) shows the Nyquist plot of three-electrode measurement and inset shows its equivalent circuit with ESR (R_1) and Rct values of 1.34 Ω and 0.296 Ω respectively by using ZFIT fitting programme v11.02. The circuit diagram presents the solution resistance R_1 in series with a branch that consists real capacitance Q_1 that is in parallel with charge transfer resistance R_2 and in parallel with a branch that consists of additional capacitance C_3 that is parallel with load Resistance R_3. Figure S3 (a-d) shows the plots of GCD curves of various electrodes for negative potentials in three-electrode measurement, the same approach was also adopted for various electrodes, tested in positive potentials as shown in Figure S4 (a-d). Figure S5 (a,b) displays specific capacitance against specific current of the various electrodes for negative and positive potentials in 2.5 M KNO_3 electrolyte solution. Figure S6 (a-d) shows the detailed cyclic voltammetry (CV) and galvanostatic charge discharge (GCD) plots of ACC 600 °C sample, tested in 2.5 M KNO_3 electrolyte in both positive and negative potential windows at different scan rates and specific currents. The material obviously shows rectangular CV and triangular GCD at both potential windows (positive and negative) in 2.5 M KNO_3 electrolyte. Previous research had indicated that the conductivity, electrolyte pH value, ionic mobility and hydration sphere radius of KNO_3 are unique qualities that are responsible for the good EDLC response [45,46]. Fig. S6. (e) shows the plot of specific capacitance against specific current in 2.5 M KNO_3 neutral electrolytes for both negative and positive potentials. The positive and negative values of capacitance at 0.5 Ag^{-1} were found to be 96 and 180 F g^{-1} respectively using equation (1). As the specific current increased to 5 Ag^{-1}, the specific capacitances were found to be still high with values of 67 and 150 F g^{-1} for positive and negative potential window, respectively. This behavior further indicated that the synthesized material possesses a good rate capability in 2.5 M KNO_3 neutral electrolyte. Hence, a symmetric device was fabricated with the neutral electrolyte.

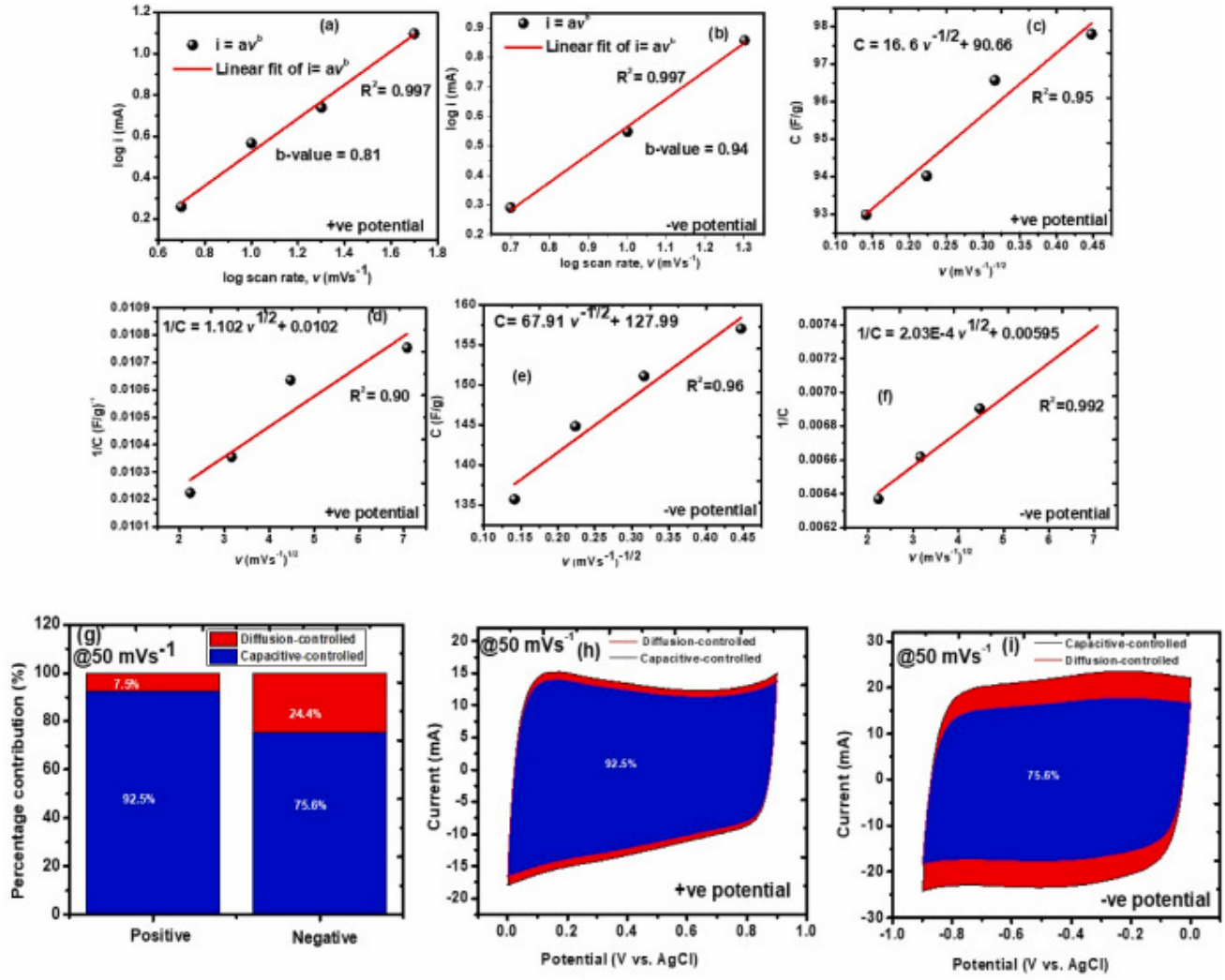

Fig. 5. (a,b) The linear relation curves between the response current and scan rates, (c,e) The linear relation curves between the response capacitive of capacitance and reciprocal square root of scan rates, (d,f) The linear relation curves between the response of total capacitance and square root of scan rates, (g) normalized contribution ratio of the capacitive and diffusion-controlled process at 50 mV s^{-1} and (h,i) CV curves at a scan rate of 50 mV s^{-1} for positive and negative electrode.

The R^2 value of 0.997 was revealed for both the anodic and cathodic processes in the i-$\upsilon^{1/2}$ plot, which is very close to 1 and suggests excellent electrochemical reversibility and capacitive characteristics of the as-synthesized material (see Fig. 5 (a & b)). The b values of negative and positive electrodes were calculated to be 0.94 and 0.81 respectively. The estimated b-values were close to 1, suggesting that the capacitive controlled process was dominant in both negative and positive electrodes which described the mechanism of energy storage of activated carbon materials as non-faradaic reaction. However, when the value of b was close to 0.5, it indicated that the diffusion-controlled Faraday process was the main electrochemical reaction mechanism for generating capacitance [36]. The EDLC capacitances of negative and positive electrode were determined from the intercept of graphs (see Fig. 5(c–e)) as 127 F g^{-1} and 90.66 F g^{-1} respectively. The total capacitances of the negative and positive electrodes were determined from the reciprocal of the intercept of the graphs (see Fig. 5(d–f)) as 168 F g^{-1} and 98 F g^{-1} respectively. Hence, the percentage contribution of capacitive and diffusion-controlled effect as 92.4732% and 7.5268% for positive electrode while the negative electrode possesses

75.565% and 24.435% at scan rate of 50 mVs^{-1}. The electrochemical mechanism of the electrodes is fully represented in Fig. 5(h–i). It was observed that the percentage contribution of diffusion-controlled effect in Fig. 5i is higher at negative electrode than positive electrode in Fig. 5h, which advantageously contributed to the generated capacitance of the electrode. During the testing of electrode in three electrode configurations by using 2.5 M KNO_3 neutral electrolyte, K^+ moves towards the negative electrode while NO_3^- accumulates ion towards positive electrode. However, the hydrated ion size of K^+(3.31 Å) is smaller than NO_3^- (3.35 Å). Thus, K^+ can move faster than NO_3^- towards electrode with less resistance, storing more charge [34]. The contribution of Alkali metal (Potassium (K^+)) in the electrolyte gives rise to high pseudocapacitive value in the negative potential during electrochemical testing.

Fig. 6(a–f) shows the electrochemical properties of symmetric device. In Fig. 6 (a), cyclic voltammetric curves of symmetric (ACC 600ºC) device were measured at various scan rates between 5 and 100 mV s^{-1} with cell potential of 1.8 V. Fig. 6 (b) shows GCD profiles of the full device at various specific currents. The discharge time obtained via the area under the GCD curves was used to determine gravimetric capacitance of the single electrode using equation (2). At specific current 0.5 A g^{-1}, the gravimetric capacitance was reported as 168 F g^{-1} and still retained about one third (67 F g^{-1}) of its original value when higher specific current of 10 A g^{-1} was applied. It is noticed that the GCD and CV curves are triangular and rectangular, respectively, which is consistent with the electrical double layer capacitor (EDLC) feature of symmetric activated carbon devices [5,15]. Ragone plot of electrodes made from biomass carbon found in previously published reports as shown in Fig. 6 (c) at different current densities, and this work produced maximum specific energy and power of 19 W h kg^{-1} and 453 W kg^{-1} respectively as compared to others. Fig. 6 (d) shows the Nyquist plot of the device, and inset shows an enlarge image of high frequency region of experimental line in Fig. 6d with ESR and Rct values of 2.09 Ω and 0.718 Ω respectively. With the comparable circuit displayed in the inset of Fig. 6e, estimated values of ESR and Rct in the Nyquist plot was 2.095 Ω and 0.925 Ω respectively. A representative circuit diagram for the device is presented in the inset of Fig. 6 (e). The circuit diagram presents the solution resistance R_1 in series with a branch that consists real capacitance Q_1 that is in parallel with charge transfer resistance R_2 and in parallel with a branch that consists of additional real capacitance Q_2 that is parallel with load Resistance R_3 and mass capacitance Q_3. The two final branches signify the middle and low frequency region, respectively. Fig. 6 (f) shows a coulombic efficiency (equation (5)) and capacitance retention of the activated carbon after 10000 cycles. The coulombic efficiency of the device is 99.6% after 10000 cycles with 72% capacitance retention. This validates the good stability of the activated carbon in neutral electrolyte (2.5 M KNO_3). Plate 1 shows the test of symmetric device for practical application.

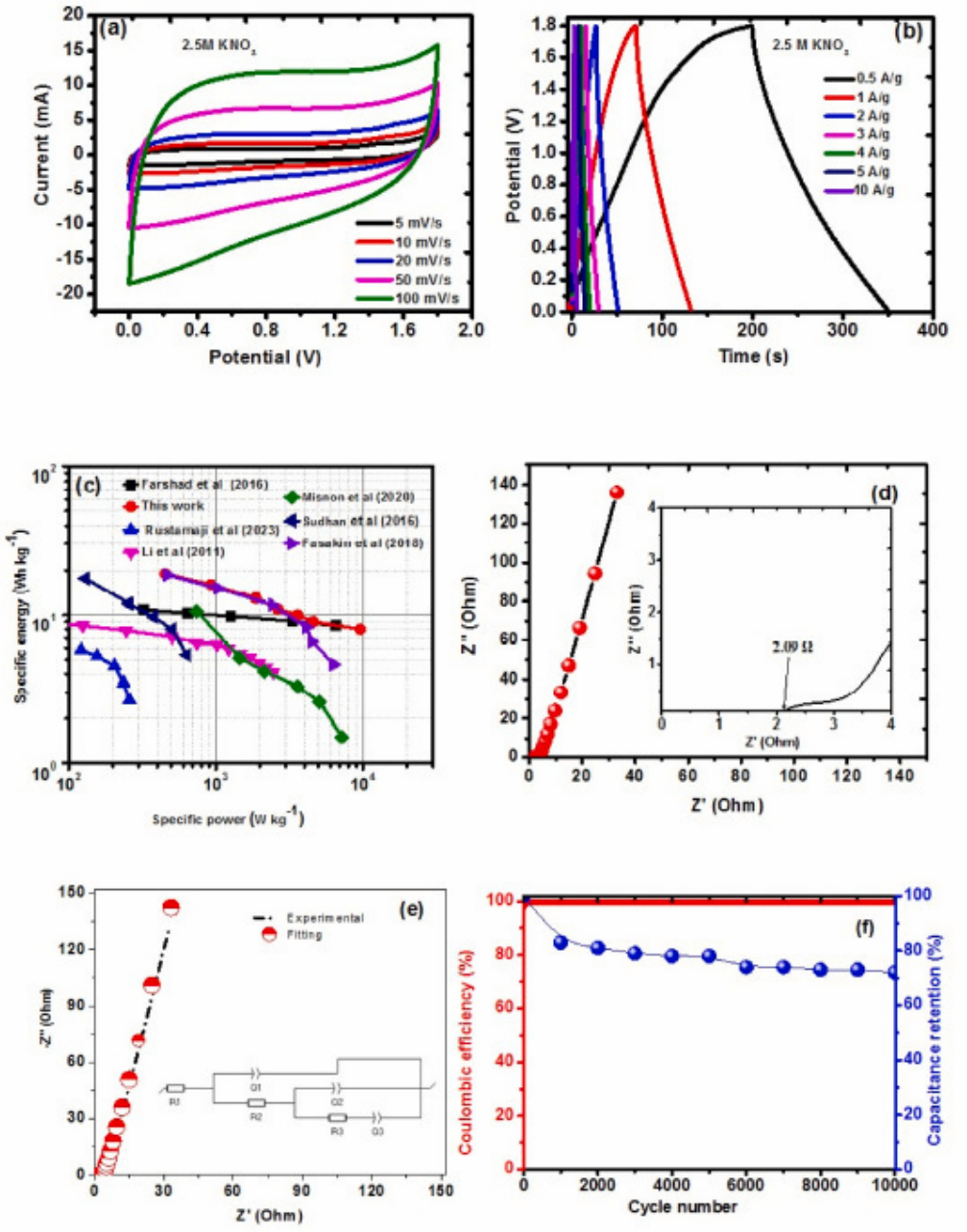

Fig. 6. (a) plots of CV at different scan rates, (b) plot of GCD at different specific currents, respectively, (c) Ragone plot of electrodes made from biomass carbon found in previously published reports as shown in Table 2. (d) Nyquist plot and inset of Fig. 6d at higher frequency (e) equivalent circuit used to fit the EIS data in Fig. 6(d) and (f) plot of coulombic efficiency and capacitance retention against cycles at 5 A g^{-1}.

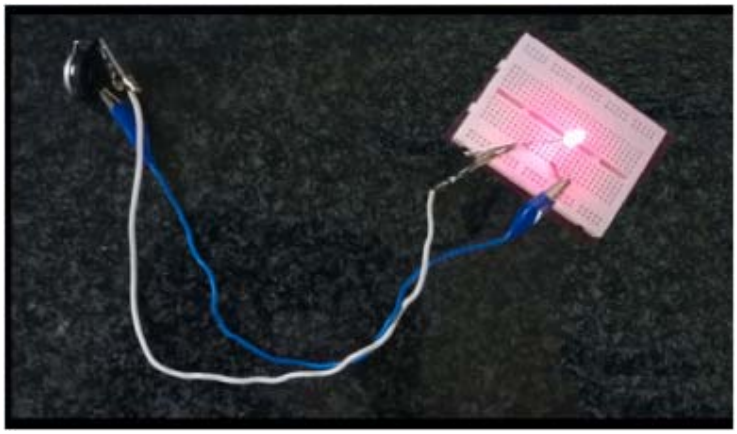

Plate 1. Test of symmetric device for practical application.

4. Conclusion

Summarily, sponge-like, amorphous and porous activated carbon is synthesized from a common waste biomass material (cocoa pod husks) at a low temperature of 600 °C. Trasatti method is adopted to verify the storage mechanism of the activated carbon material (ACC 600 °C) with the percentage contribution of capacitive and diffusion-controlled effect as 92.4732% and 7.5268% for positive electrode while the negative electrode possesses 75.565% and 24.435% at scan rate of 50 mVs^{-1}. The ACC 600°C device exhibits higher specific capacitance values of 168 Fg^{-1} with corresponding S.E and S.P of 19 Wh kg^{-1} and of 453 W kg^{-1} at 0.5 A g^{-1}, which shows a better S.E and moderate S.P. Most importantly, the device is still stable in 2.5 M KNO_3 aqueous electrolyte despite being subjected to 10000 cycles. However, the results obtained in this work provide a mild route with cheap and abundant waste material (Cocoa pod husks) to synthesize high quality activated carbon and design a much stable device, by using less toxic electrolyte and electrode (waste) materials.

CRediT authorship contribution statement

Oladepo Fasakin: Writing – review & editing, Writing – original draft, Methodology, Investigation, Formal analysis, Data curation, Conceptualization. **Kabir O. Oyedotun:** Writing – review & editing, Writing – original draft, Methodology, Formal analysis. **Abdulmajid A. Mirghni:** Writing – review & editing, Formal analysis, Data curation. **Ndeye F. Sylla:** Writing – review & editing, Formal analysis, Data curation. **Badr A. Mahmoud:** Writing – review & editing, Data curation, Conceptualization. **Ncholu Manyala:** Writing – review & editing, Supervision, Resources, Conceptualization.

Declaration of competing interest

The authors declare that they have no known competing financial interests or personal relationships that could have appeared to influence the work reported in this paper.

Acknowledgements

Dr. O. Fasakin deeply appreciates TETFUND with grant number TETF/DASTD/UNI/OSUN/TSAS/2022, for funding his postdoctoral fellowship. He is also

very grateful to Obafemi Awolowo University in Ile-Ife for releasing him to participate in the postdoctoral programme.

Data availability

Data will be made available on request.

References

1) C.O. Okeh, C.O. Onwosi, F.J.C. Odibo, Biogas production from rice husks generated from various rice mills in Ebonyi State, Nigeria, Renew. Energy, 62 (2014), pp. 204-208, 10.1016/j.matpr.2018.11.072
2) A. Bello, N. Manyala, F. Barzegar, A.A. Khaleed, D.Y. Momodu, J. Dangbegnon, Renewable pine cone biomass derived carbon materials for supercapacitor application, RSC Adv., 6 (2016), pp. 1800-1809, 10.1039/C5RA21708C
3) Y. Sun, Q. Wu, G. Shi, Graphene-based new energy materials, Energy Environ. Sci., 4
4) A.F. Ghoniem, Needs Resources and climate change: clean and efficient conversion technologies, Prog. Energy Combust. Sci., 37 (2011), pp. 15-51, 10.1016/j.pecs.2010.02.006
5) T.S. Mathis, N. Kurra, X. Wang, D. Pinto, P. Simon, Y. Gogotsi, Energy storage data reporting in perspective-Guidelines for interpreting the performance of electrochemical energy storage systems, Adv. Energy Mater., 9 (39) (2019), pp. 1902007-1902016, 10.1002/aenm.20190200
6) B.E. Conway, Electrochemical Supercapacitors: Scientific Fundamentals and Technological Applications, Springer, 1999. ISBN 978-1-4757-3058-6.
7) P. Simon, Y. Gogotsi, Materials for electrochemical capacitors, Nat. Mater., 7 (2008), pp. 845-854, 10.1038/nmat2297
8) Y. Zhai, Y. Dou, D. Zhao, P.F. Fulvio, R.T. Mayes, S. Dai, Carbon materials for chemical capacitive energy storage, Adv. Mater. (Weinheim, Ger.), 23 (42) (2011), pp. 4828-4850, 10.1002/adma.201100984
9) S. Dörfler, I. Felhösi, T. Marek, S. Thieme, H. Althues, L. Nyikos, S. Kaskel, High power supercapacitor electrodes based on vertical aligned carbon nanotubes on aluminium, J. Power Sources, 227 (2013), pp. 218-228, 10.1016/j.jpowsour.2012.11.068
10) E. Iyyamperumal, S. Wang, L. Dai, Vertically aligned BCN nanotubes with high capacitance, American Chemical Society Nano, 6 (6) (2012), pp. 5259-5265, 10.1021/nn301044v
11) Y. Korenblit, M. Rose, E. Kockrick, L. Borchardt, A. Kvit, S. Kaskel, G. Yushin, High-rate electrochemical capacitors based on ordered mesoporous silicon carbide-derived carbon, American Chemical Society Nano, 4 (3) (2010), pp. 1337-1344, 10.1021/nn901825y
12) P. Simon, Y. Gogotsi, Capacitive energy storage in nanostructured carbon–electrolyte systems, Accounts Chem. Res., 46 (2013), pp. 1094-1103, 10.1021/ar200306b
13) Y. Gao, Y.S. Zhou, M. Qian, X.N. He, J. Redepenning, P. Goodman, H.M. Li, L. Jiang, Y.F. Lu, Chemical activation of carbon nano-onions for high-rate supercapacitor electrodes, Carbon, 51 (2013), pp. 52-58, 10.1016/J.Carbon.2012.08.009

14) B.G. Choi, M. Yang, W.H. Hong, J.W. Choi, Y.S. Huh, 3D macroporous graphene frameworks for supercapacitors with high energy and power densities, American Chemical Society Nano, 6 (5) (2012), pp. 4020-4027, 10.1021/nn3003345
15) L.L. Zhang, R. Zhou, X.S. Zhao, Graphene-based materials as supercapacitor electrodes, J. Mater. Chem., 20 (2010), pp. 5983-5992, 10.1039/C000417K
16) X. Jiang, F. Guo, X. Jia, S. Liang, Kuangye Peng, Lin Qian, Synthesis of biomass-based porous graphitic carbon combining chemical treatment and hydrothermal carbonization as promising electrode materials for supercapacitors, Ionics, 26 (2020), pp. 3655-3668, 10.1007/s11581-020-03487-8
17) V.N. Kitenge, K.O. Oyedotun, O. Fasakin, D.J. Tarimo, N.F. Sylla X. Van Heerden N Manyala, Enhancing the electrochemical properties of a nickel cobalt-manganese ternary hydroxide electrode using graphene foam for supercapacitors applications, Materials for Renewable and Sustainable Energy, 10 (2021), pp. 1-16, 10.1007/s40243-021-00192-y
18) D. Momodu, N.F. Sylla, B. Mutuma, A. Bello, T. Masikhwa, S. Lindberg, A. Matic, N. Manyala, Stable ionic-liquid-based symmetric supercapacitors from Capsicum seed-porous carbons, J. Electroanal. Chem., 838 (2019), pp. 119-128, 10.1016/j.jelechem.2019.02.045
19) V. Subramanian, C. Luo, A.M. Stephan, K.S. Nahm, S. Thomas, B. Wei, Supercapacitors from activated carbon derived from banana fibers, J. Phys. Chem. C, 111 (2007), pp. 7527-7531, 10.1021/jp067009t
20) X.Y. Zhang, B.K. Sun, X. Fan, P. Liang, G.M. Zhao, B.K. Saikia, X.Y. Wei, Hierarchical porous carbon derived from coal and biomass for high performance supercapacitors, Fuel, 311 (2022), pp. 122552-122559, 10.1016/j.fuel.2021.122552
21) R. Nasser, J. Tiantian, J.M. Song, Hierarchical porous activated carbon derived from olives: preparation, (N, S) co-doping, and its application in supercapacitors, J. Energy Storage, 51 (2022), pp. 104348-104360, 10.1016/j.est.2022.104348
22) 2D porous carbon nanosheet derived from turnip: preparation, Characterization and its electrochemical performance, J. Energy Storage, 59 (2023), pp. 106552-106563, 10.1016/j.est.2022.106552
23) N. Venkatesan, T. Kesavan, M. Raja, K. Ramanujam, N.N. Fathima, Efficient electrochemical performance of nitrogen-doped porous activated carbon for high energy symmetric pouch cell supercapacitors, J. Energy Storage, 55 (2022), pp. 105698-105709, 10.1016/j.est.2022.105698
24) X. He, P. Ling, M. Yu, X. Wang, X. Zhang, M. Zheng, Rice husk-derived porous carbons with high capacitance by $ZnCl_2$ activation for supercapacitors, Electrochim. Acta, 105 (2013), pp. 635-641, 10.1016/j.electacta.2013.05.050
25) C.A. Forero-nuñez, J. Jochum, F.E. Sierra, Effect of particle size and addition of cocoa pod husk on the properties of sawdust and coal pellets, Ing. Invest., 35 (1) (2019), pp. 17-23, 10.15446/ing.investig.v35n1.46157
26) G. Kilama, P.O. Lating, J. Byaruhanga, S. Biira, Quantification and characterization of cocoa pod husks for electricity generation in Uganda, Energy, Sustainability and Society, 9 (2019), pp. 22-32, 10.1186/s13705-019-0205-4
27) W. Tsai, Y. Bai, Y. Lin, Y. Lai, C. Tsai, Porous and adsorption properties of activated carbon prepared from cocoa pod husk by chemical activation, Biomass Conversion and Biorefinery, 10 (2020), pp. 35-43, 10.1007/s13399-019-00403-7
28) O.A.A. Eletta, A.G. Adeniyi, J.O. Ighalo, D.V. Onifade, F.O. Ayandele, Valorisation of cocoa (Theobroma cacao) pod husk as precursors for the production of adsorbents for water treatment, Environmental technology reviews, 9 (2020), pp. 20-36, 10.1080/21622515.2020.1730983

29) N. Karic, A.S. Maia, A. Teodorović, N. Atanasova, G. Langergraber, G. Crini, A.R.L. Ribeiro, M. Dolić, Bio-waste valorization, Agricultural wastes as biosorbents for removal of (in)organic pollutants in wastewater treatment, Chemical Engineering Journal Advances, 9 (2022), pp. 100239-100245, 10.1016/j.ceja.2021.100239
30) A.A. Mirghni, K.O. Oyedotun, B.A. Mahmoud, O. Fasakin, D.J. Tarimo, Ncholu Manyala, A study of Co-Mn phosphate supported with graphene foam as promising electrode materials for future electrochemical capacitors, Int. J. Energy Res., 46 (3) (2021), pp. 3080-3094, 10.1002/er.7365
31) K.O. Oyedotun, A.A. Mirghni, O. Fasakin, D.J. Tarimo, V.N. Kitenge, N. Manyala, High-energy asymmetric supercapacitor based on the nickel cobalt oxide (NiCo2O4) nanostructure material and activated carbon derived from cocoa pods, Energy Fuels, 35 (24) (2021), pp. 20309-20319, 10.1021/acs.energyfuels.1c02560
32) K.M. Rambau, D.J. Tarimo, O. Fasakin, N.M. Musyoka, N. Manyala, Asymmetric supercapacitor based on novel coal fly ash derived metal–organic frameworks as positive electrode and its derived carbon as negative electrode, J. Appl. Electrochem., 52 (5) (2022), pp. 821-834, 10.1007/s10800-022-01672-3
33) B.A. Mahmoud, A.A. Mirghni, K.O. Oyedotun, O. Fasakin, N. Manyala, Nanoplatelets ammonium nickel-cobalt phosphate graphene foam composite as novel electrode material for hybrid supercapacitors, J. Alloys Compd., 883 (2021), pp. 160897-160907, 10.1016/j.jallcom.2021.160897
34) O. Fasakin, J.K. Dangbegnon, D.Y. Momodu, M.J. Madito, K.O. Oyedotun, M.A. Eleruja, N. Manyala, Synthesis and characterization of porous carbon derived from activated banana peels with hierarchical porosity for improved electrochemical performance, Electrochim. Acta, 262 (2018), pp. 187-196, 10.1016/j.electacta.2018.01.028
35) R. Nasser, H. Zhou, A.B.G. Trabelsi, F.H. AlKallas, H. Elhouichet, J. Song, Engineering preparation of the nanocomposite containing $CoWO_4$ nanodots and its high electrochemical activities, J. Energy Storage, 68 (2023), pp. 107763-107773, 10.1016/j.jpcs.2021.110500
36) T. Jiang, X. Wang, H. Zhou, R. Nasser, D. Wu, H. Zhou, J. Song, Preparation of lily based porous carbon loaded NiCo double hydroxide nanosheets complementary composite, its application in all-solid-state asymmetric supercapacitors, J. Energy Storage, 72 (2023), pp. 108184-1018193, 10.1016/j.est.2023.108184
37) C. Zou, D. Wu, M. Li, Q. Zeng, F. Xu, Z. Huang, R. Fu, Template-free fabrication of hierarchical porous carbon by constructing carbonyl crosslinking bridges between polystyrene chains, J. Mater. Chem., 20 (2010), pp. 731-735, 10.1039/B917960G
38) Y. Mao, H. Duan, B. Xu, L. Zhang, Y. Hu, C. Zhao, Z. Wang, L. Chen, Y. Yang, Lithium storage in nitrogen-rich mesoporous carbon materials, Energy Environ. Sci., 5 (2012), pp. 7950-7955, 10.1039/C2EE21817H
39) L. Yao, G. Yang, P. Han, Z. Tang, J. Yang, Three-dimensional beehive-like hierarchical porous polyacrylonitrile-based carbons as high-performance supercapacitor electrodes, J. Power Sources, 315 (2016), pp. 209-217, 10.1016/j.jpowsour.2016.03.006
40) Y. Wang Y, X. Duan, L. Liang, R. Tang, S. Sun, H. Wang Wei, P. Huang, H. Yang, Hu hierarchical porous activated carbon derived from coconut shell for ultrahigh-performance supercapacitors, Molecules, 28 (20) (2023), pp. 7187-7200, 10.3390/molecules28207187
41) M.S. Yerdauletov K, B. Nazarov, M.A. Mukhametuly, C. Yeleuov, R. Daulbayev, A. Abdulkarimova, F. Yskakov, V. Krivchenko Napolskiy, Characterization of activated

carbon from rice husk for enhanced energy storage devices, Molecules, 28 (2023), pp. 5818-5829, 10.3390/molecules28155818
42) A. Ahmad M, A. Gondal, M. Hassan, R. Iqbal, S. Ullah, A.S. Alzahrani, W.A. Memon, F. Mabood, S. Melhi, Preparation and characterization of physically activated carbon and its energetic application for all-solid-state supercapacitors: a case study, American Chemical Society Omega, 8 (2023), pp. 21653-21663, 10.1021/acsomega.3c01065
43) K.O. Oyedotun, F. Barzegar, A.A. Mirghni, A.A. Khaleed, T.M. Masikhwa, N. Manyala, Examination of high porosity activated carbon obtained from dehydration of white sugar for electrochemical capacitor applications, ACS Sustain. Chem. Eng., 7 (2018), pp. 537-546, 10.1021/acssuschemeng.8b04080
44) D. Momodu, M. Madito, F. Barzegar, A. Bello, A. Khaleed, O. Olaniyan, J. Dangbegnon, N. Manyala, Activated carbon derived from tree bark biomass with promising material properties for supercapacitors, J. Solid State Electrochem., 21 (2017), pp. 859-872, 10.1007/s10008-016-3432-z
45) F. Barzegar, D.Y. Momodu, O.O. Fashedemi, A. Bello, J.K. Dangbegnon, N. Manyala, Investigation of different aqueous electrolytes on the electrochemical performance of activated carbon-based supercapacitors, RSC Adv., 5 (2015), pp. 107482-107487, 10.1039/C5RA21962K
46) M. Toupin, D. Bélanger, I.R. Hill, D. Quinn, Performance of experimental carbon blacks in aqueous supercapacitors, J. Power Sources, 140 (2005), pp. 203-210, 10.1016/j.jpowsour.2004.08.014
47) X. Li, W. Xing, S. Zhou, J. Zhou, F. Li, S.Z. Qiao, G.Q. Lu, Preparation of capacitor's electrode from sunflower seed shell, Bioresour. Technol., 102 (2011), pp. 1118-1123, 10.1016/j.biortech.2010.08.110
48) H. Rustamaji, T. Prakoso, H. Devianto, P. Widiatmoko, K.A. Kurnia, Facile synthesis of N, S-modified activated carbon from biomass residue for promising supercapacitor electrode applications, Bioresour. Technol. Rep., 21 (2023), pp. 101301-101309, 10.1016/j.biteb.2022.101301
49) N. Sudhan, K. Subramani, M. Karnan, N. Ilayaraja, M. Sathish, Biomass-derived activated porous carbon from rice straw for a high-energy symmetric supercapacitor in aqueous and nonaqueous electrolytes, Energy Fuels, 31 (2017), pp. 977-985, 10.1021/acs.energyfuels.6b01829
50) F. Barzegar, A.A. Khaleed, F.U. Ugbo, K.O. Oyeniran, D.Y. Momodu, A. Bello, J.K. Dangbegnon, N. Manyala, Cycling and floating performance of symmetric supercapacitor derived from coconut shell biomass, AIP Adv., 6 (2016), pp. 115306-115314, 10.1063/1.4967348
51) I.I. Misnon, N.K.M. Zain, T.S. Lei, Activated carbon with graphitic content from stinky bean seedpod biowaste as supercapacitive electrode material, Ionics, 26 (2020), pp. 4081-4093, 10.1007/s11581-020-03565-x
52) B. Shaku, T.P. Mofokeng, N.J. Coville, K.I. Ozoemena, M.S. Maubane-Nkadimeng, Biomass valorisation of marula nutshell waste into nitrogen-doped activated carbon for use in high performance supercapacitors, Electrochim. Acta, 442 (2023), pp. 141828-141840, 10.1016/j.electacta.2023.141828